Robotica (2018) volume 36, pp. 1613–1626. © Cambridge University Press 2018
doi:10.1017/S0263574718000590

Kinematic study on a self-propelled bionic underwater robot with undulation and jet propulsion modes

Ou Xie†,*, Qixin Zhu†, Lin Shen‡, Kun Ren†

†*School of Mechanical Engineering, Suzhou University of Science and Technology, Suzhou 215009, P.R. China. E-mails: bob21cn@163.com, renkun2353@163.com*
‡*Transmatic Precision Metal Forming (Suzhou) Co., Ltd., Suzhou 215129, P.R. China. E-mail: she_nling@126.com*

(Accepted June 30, 2018. First published online: July 30, 2018)

SUMMARY
This paper proposed a novel type of bionic underwater robot (BUR). The undulation and jet propulsion modes on the self-propelled BUR were combined, and the kinematic characteristics of the two propulsion modes were thoroughly compared. First, the prototype and swimming strategy of the BUR were presented, and a dynamic model of the BUR was established based on several assumptions. Then, a central pattern generator (CPG) model allowing free adjustment of frequency and amplitude was employed to achieve the undulation propulsion of carangiform fish and the jet propulsion of jellyfish. Also, the kinematic characteristics of the two propulsion modes were investigated through experiments under different caudal fin actuation parameters. The experimental results indicate that the developed prototype can realize the undulation and jet propulsion by the means of the coordinated movement of the multi-caudal fins. By adjusting the CPG parameters, the BUR can switch the propulsion mode smoothly. Furthermore, the propulsion velocity of the BUR initially increased rapidly with the frequency and then slowed down when the frequency was greater than 0.8 Hz in both propulsion modes. The undulation propulsion velocity increased with the amplitude in the measurement ranges, however, the jet propulsion velocity initially increased quickly with the amplitude and then kept constant and even decreased when the amplitude was greater than 11 cm. Under the same caudal fin actuation parameters, the average velocity in undulation propulsion mode was higher than that in jet propulsion mode.

KEYWORDS: Bionic underwater robot (BUR), undulation propulsion mode, jet propulsion mode, kinematics

1. Introduction

Underwater robots have recently been used in several applications.[1,2] Various applications, such as military defense and marine protection, require high-performance autonomous underwater vehicles (AUVs), especially for propulsion efficiency and maneuverability. Due to the limitation of the structure and propulsion mechanism, traditional rotary propeller propulsion mode has various defects, which severely restrict the application of the conventional AUVs.[3] As a type of AUV, biomimetic underwater robots have been one of the areas of interest in recent years.[4–6] By borrowing the structures and sensory mechanisms of aquatic organisms, engineers seek to design different types of bio-inspired underwater robots.

In nature, most of aquatic organisms employ jet or undulation propulsion mode as their swimming mode.[7] Aquatic organisms with undulation propulsion mode are featured by high swimming efficiency, strong maneuverability and low noise.[8] In comparison, the jet propulsion mode has the merits of providing greater instantaneous thrust in a short time, good accelerating performance and strong environment adaptability.[9] Researchers have studied these two propulsion modes by the means of

* Corresponding author: E-mail: hnxieou@126.com

https://doi.org/10.1017/S0263574718000590 Published online by Cambridge University Press

theoretical modeling,[10−12] numerical simulation,[13−15] morphology and kinematic study,[17−19] and various BURs are developed inspired by real aquatic organisms directly.[20−23] However, all works mentioned above are limited to mimic a single propulsion mode or body structure of the aquatic organisms. It can only accomplish limited tasks in a specific under water environment, for instance, AUVs with undulation propulsion mode only suitable for cruising task while jet propulsion AUVs just showed a good ability for rapid flee dangers, which cannot meet the requirements of the complex under water operations.

Inspired by aquatic organisms, we proposed a novel type of bionic underwater robot (BUR) which organically combines the undulation propulsion mode and jet propulsion mode. It has the merits of the two propulsion modes and more suitable for complex marine environment. The BUR can achieve a serial of motions: undulating, jetting, turning, submerging, emerging and braking. In view of the intrinsic characteristics of rhythm, coordination and variety, central pattern generators (CPGs) are well suited to tackling multiple articulated joints or degrees of freedom (DOFs) related to locomotion control. In practical engineering, various robots with rhythmic locomotion are controlled by CPGs.[24,25] Contrary to the body wave-based approach (i.e., sine-based approach) commonly utilized in fish-like swimming control, CPG-based control has the advantages of online gait generation and smooth trajectory transition, and the control signals are relatively simple.[26,27] This paper aims to combine the undulation propulsion mode and jet propulsion mode through the CPG-based method and thoroughly compare the kinematics of the two modes through the self-propelled BUR.

The rest of this paper is organized as follows. The overall physical design and swimming strategy of the BUR are briefly overviewed in Section 2. Section 3 establishes the dynamic model of the BUR. In Section 4, the CPG-based model and its control methods applied to undulation propulsion mode and jet propulsion mode are elaborated in detail. Section 5 tests the linear swimming velocity and discusses the comparative results. Finally, Section 6 concludes the work with some recommendations made for future work.

2. Physical Design

2.1. Prototype

Jellyfish swimming is a typical jet propulsion movement, which generates thrust by rapid shrinking the umbrella-like body. As shown in Fig. 1(a), Bajcar et al.[17] pointed that the swimming process of the jellyfish can be divided into the following stages: expanding lumen, sucking water, rapidly shrinking lumen and spraying water.

Fish are widely distributed aquatic organism with multiple types and large quantity. According to the propulsive structure, the swimming mode of fish can be divided into two categories: Body and/or Caudal Fin (BCF), and Median and/or Paired Fin (MPF).[28,29] The swimming mode of carangiform fish can be classified into the BCF mode. As shown in Fig. 1(b), carangiform fish undulates the last half or third of their bodies in transverse direction to generate thrust force.

Inspired by the morphology and kinematics of both carangiform fish and jellyfish, a novel type of BUR was proposed. As shown in Fig. 1(c) and (d), the BUR consists of a head cabin and four caudal fins. A missile-like streamlined contour is introduced for the design of head cabin, which is made of acrylonitrile butadiene styrene (ABS) resin and printed by rapid prototyping according to the 3-D model design. Various function units, such as control board, proximity sensor, tilt sensor and large capacity lithium battery array, are encapsulated in the head cabin. The four caudal fins are installed at equiangular intervals, around the circumference of the head cabin baseboard. This installation method is beneficial to counteract the lateral force generated by caudal fins and avoid the head-shaking problem. The caudal fin is composed of two joints and a flexible fin with large aspect ratio, which imitates the last half body of the carangiform fish. The joints driven by servomotors, and each servomotor is sealed independently. The technical parameters of the BUR prototype are listed in Table I.

2.2. Swimming strategy

By the means of the coordinate movement of the multi-caudal fins, the BUR can accomplish a series of maneuver motions. As shown in Fig. 2(a), when the four caudal fins undulate simultaneously and the face-to-face installed caudal fins have the phase difference of 180°, the BUR can achieve the

https://doi.org/10.1017/S0263574718000590 Published online by Cambridge University Press

Table I. Technical specifications of the BUR prototype.

Item	Characteristics
Dimension($L \times W \times H$)	600 × 170 × 170 (mm)
Total mass	5.5 (kg)
Numbers of the caudal fins	4
Length of the oscillation part	280 (mm)
Drive mode	DC servomotors
On-board sensors	3 infrared sensors
Operation voltage	DC 7.4 (V)

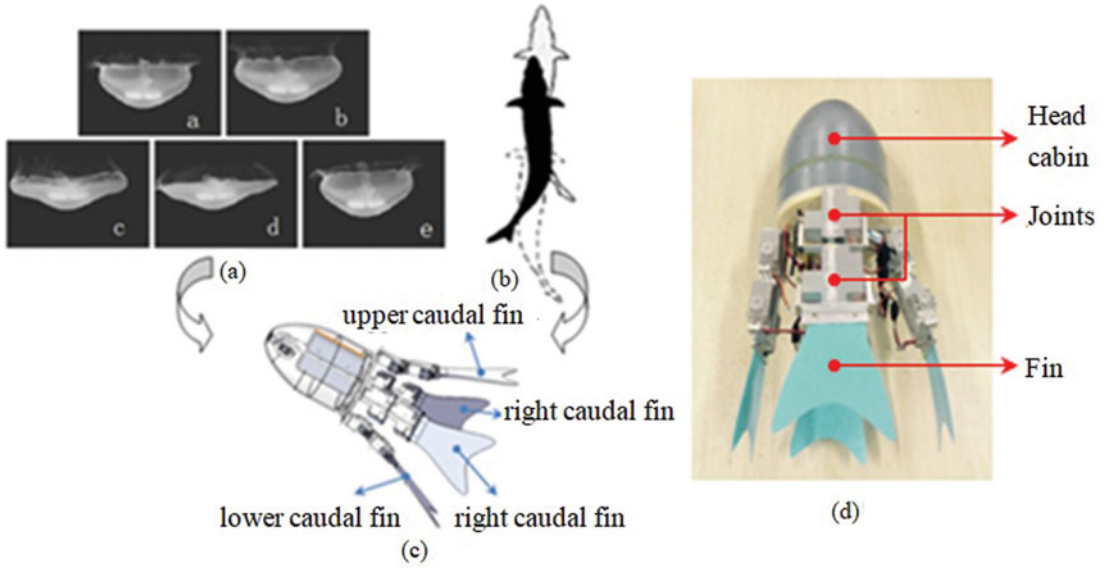


Fig. 1. Mechanical design of the developed BUR. (a) Jellyfish swimming process. (b) Carangiform fish swimming process. (c) Concept design. (d) BUR prototype.

undulation propulsion mode. Jet propulsion mode (as shown in Fig. 2(b)) is that the four caudal fins slowly open and then flap rapidly and simultaneously. A backward high-speed compressed water flow is formed, which can provide a large forward thrust to the BUR. According to the motion features of the jellyfish, the jet propulsion movement of the BUR can be divided into two stages: outspread fins stage and fold fins stage. In the swimming period, the speed of fold fins movement should be higher than that of outspread fins movement so as to form a large jet propulsion force. Figure 2(c) shows the braking actions. When the BUR moves forward, the four caudal fins rapidly open to the maximum angle simultaneously and then keep still. The BUR suffers a large hydraulic resistance and stops quickly. After that the caudal fins return to straight slowly. As shown in Fig. 2(d), (e) and (f), when a pair of face-to-face installed caudal fins deflects a large angle in a random direction (up, down, left or right) the BUR will suffer a large torque in this direction simultaneously. Accordingly the turning, submerging or emerging actions are accomplished, respectively.

3. Dynamic Modeling of the BUR

Based on the analysis on structure and kinematics in previous section, a simplified mechanical model of the BUR was established. As shown in Fig. 3, the caudal fin and caudal peduncle were simplified as two rigid bar J_1 and J_2. Driven by the caudal peduncle J_2, the caudal fin J_1 flaps in the HH' direction, which is perpendicular to the movement direction of the BUR. The flapping displacement is represented as h. v_a and h_0 indicate the flapping speed and flapping amplitude, respectively. Meanwhile, the caudal fin swings around the joint O to form an attack angle α, and the swing amplitude of the caudal fin is α_0. Several assumptions are proposed for modeling: First, the BUR is always fixed in the water and

https://doi.org/10.1017/S0263574718000590 Published online by Cambridge University Press

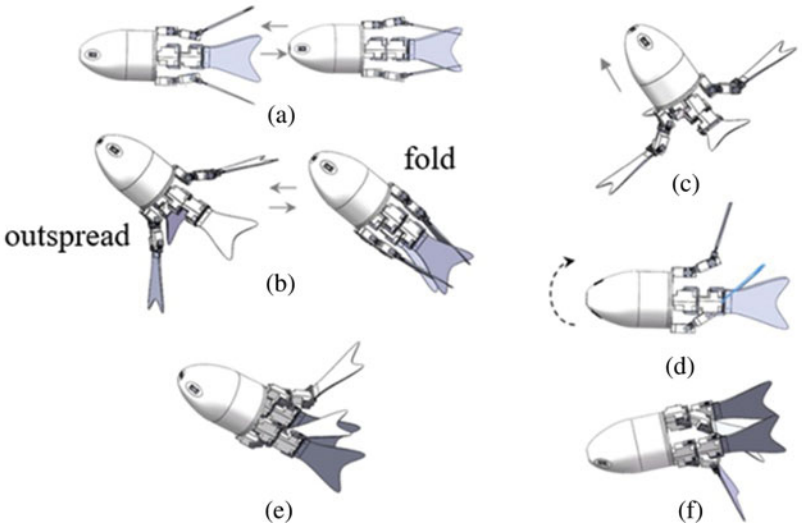


Fig. 2. Various swimming modes of BUR. (a).Undulating, (b) jetting, (c) braking, (d) turning, (e) emerging and (f) submerging.

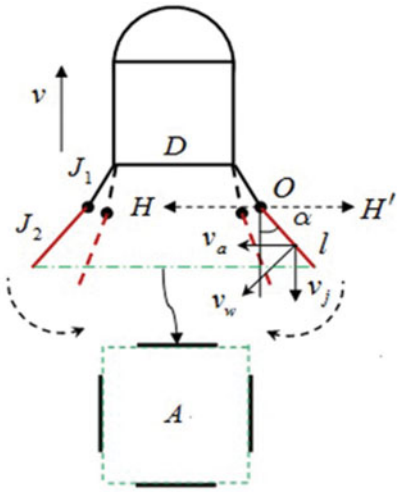


Fig. 3. Physical model of the BUR.

the initial velocity of the water is zero. Second, driven by the caudal fins, the water among the caudal fins flow with a uniform velocity v_w and its direction is perpendicular to the caudal fins.

The movement of the caudal fin can be expressed as

$$\begin{cases} h = h_0 \cos\omega t \\ \alpha = \alpha_0 \cos(\omega t - \varphi) \end{cases} \tag{1}$$

where $\omega = 2\pi f$, f is the flapping frequency and φ is the phase difference between the attack angle and swing angle.

Then, the flapping speed can be calculated by

$$v_a = \dot{h} = 2\pi f h_0 \sin(2\pi f t) \tag{2}$$

The area enclosed by the ends of the four caudal fins can be described as

$$A = (D + 2(h_0 \cos(2\pi f t) + l \sin\alpha))^2 \tag{3}$$

where D is the distance between the two face-to-face installed caudal fins.

https://doi.org/10.1017/S0263574718000590 Published online by Cambridge University Press

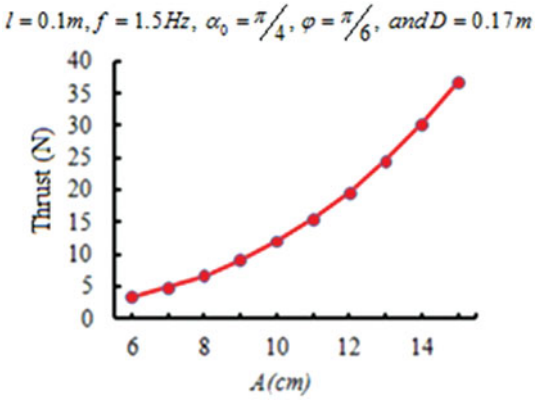


Fig. 4. The average thrust force as a function of flapping amplitude.

According to the momentum theorem, the dynamic function of the BUR can be rewritten as

$$F\Delta t = mv_j = \rho A v_j \Delta t v_j \tag{4}$$

where Δt is the time and $v_j = v_a \tan\alpha$ is the backward velocity component of water jet.m and ρ are the mass and density of the water jet, respectively.

Simplify Eq. (4), and the thrust force generated by the caudal fins can be shown as

$$F = \rho A v_j^2 \tag{5}$$

Combining Eqs. (1), (2), (3) and (5), the thrust force can be rewritten as

$$\begin{aligned} F = {} & \rho(D + 2(h_0 \cos(2\pi ft) + l \sin(\alpha_0 \cos(2\pi ft - \varphi)))^2 \\ & (2\pi f h_0 \sin(2\pi ft)\tan(\alpha_0 \cos(2\pi ft - \varphi)))^2 \end{aligned} \tag{6}$$

Furthermore, the average thrust force is defined as

$$\bar{F} = \frac{1}{T}\int_0^T F dt \tag{7}$$

where T is the movement period of the caudal fin.

Based on the dynamic functions, simulations were conducted to investigate the effects of the caudal fin actuation parameters on its average thrust force. Figures 4 and 5 show the average thrust force as a function of flapping amplitude and frequency, respectively. As can be seen, the average thrust forces generated by caudal fin increase with the caudal fin flapping amplitude and frequency.

The BUR also suffer a fluid drag when swimming in water, which can be shown as[30]

$$\bar{F}_D = \frac{1}{2}\rho C_D S_D \bar{u}^2 \tag{8}$$

where ρ is the fluid density, C_D is the flow drag coefficient, S_D is the contact area of the BUR body with the surrounding fluid medium and $\bar{u}$ is the average swimming speed of the BUR.

When the BUR keeps stability swimming, the thrust and drag forces are balanced

$$\bar{F} - \bar{F}_D = 0 \tag{9}$$

https://doi.org/10.1017/S0263574718000590 Published online by Cambridge University Press

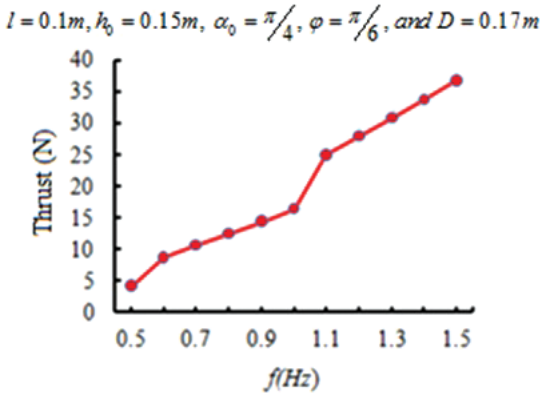


Fig. 5. The average thrust force as a function of flapping frequency.

According to Eq. (8), Eq. (9) can be rewritten as

$$\bar{u}^2 = \frac{2\bar{F}}{\rho C_D S_D} \tag{10}$$

As shown in Eq. (10), the square of the average speed is proportional to the average thrust force. Therefore, it is possible to predict that the average speed of BUR will increase with the caudal fin flapping amplitude and frequency.

4. CPG Control for BUR

4.1. CPG oscillatory units

Periodic rhythmic movements widely appear in organisms, such as breathing, heartbeat, swimming and walking. Biologists generally believe that the rhythmic movement of animals is a voluntary action in the lower nervous center, which is governed by CPG. Inspired by CPG control mode of the organisms, various CPG models have been constructed in bionic robotics. A widespread approach to model CPGs is to use dynamical systems, which are mathematically composed of coupled nonlinear oscillators and specifically weakly coupled ones. In view of the periodic rhythmic movements of the multi-caudal fins, a set of non-linear oscillators were introduced for DOFs control:[31]

$$\begin{cases} \dot{x} = -\omega y + x(m - x^2 - y^2) \\ \dot{y} = \omega x + y(m - x^2 - y^2) \end{cases} \tag{11}$$

where x and y are two state variables of the nonlinear oscillator, ω is the frequency parameter of the oscillator and m is the amplitude parameter of the oscillator.

4.2. Topology model of CPG network

Considering that each caudal fin of the BUR can be viewed as a two-link ($J_{i,}, J_{i+1}$) serial mechanism, as shown in Fig. 6, a weak coupling chain-type CPG network was established in accordance with the mechanical configuration. The CPG network consists of eight interconnected CPG units (CPG_1,...,CPG_8), each of which controls one joint actuated by a servomotor. Accordingly, based on the weak coupling single chain-type CPG mode introduced in ref. [30], a weak coupling double chain-type CPG mode for multi-caudal fins control can be described as

$$\begin{cases} \dot{x}_i = -\omega_i y_i + x_i(m_i - x_i^2 - y_i^2) + \sum_{k=1}^{i-1} h_{i,k}(x_k \cos\varphi_{i,k} + y_k \sin\varphi_{i,k}) \\ \dot{y}_i = \omega_i x_i + y_i(m_i - x_i^2 - y_i^2) + \sum_{l=i+1}^{n} h_{i,l}(x_l \sin\varphi_{i,l} + y_l \cos\varphi_{i,l}) \\ z_i = c_i y_i \end{cases} \tag{12}$$

https://doi.org/10.1017/S0263574718000590 Published online by Cambridge University Press

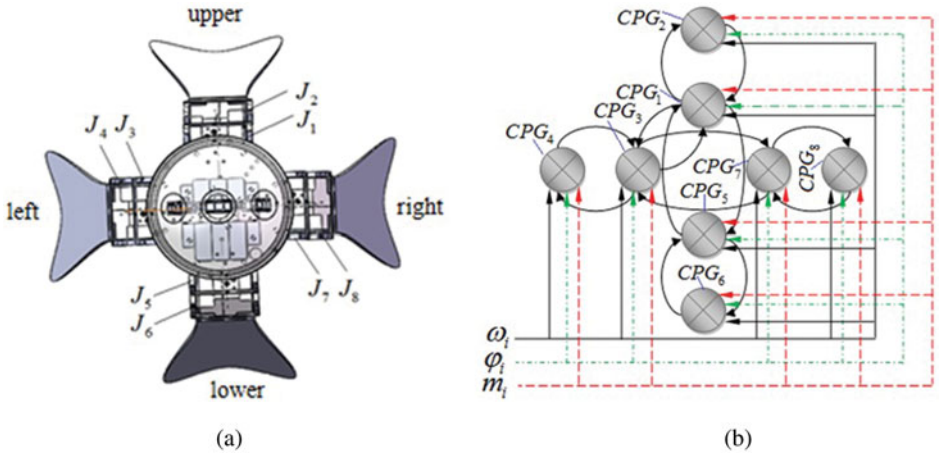


Fig. 6. Topology of the CPG network for BUR swimming control. (a) Joints configuration of the BUR. (b) CPG network.

where i=1,2,...,n, and n indicates the total number of oscillators in the CPG network. x_i is the membrane potential of the ith CPG unit. y_i is the adjusting potential. ω_i and m_i are the frequency and amplitude, respectively. $\varphi_{i,k}$ and $\varphi_{i,l}$ are the phase differences between the CPG units. $h_{i,k}$, and $h_{i,l}$ are the coupling weights determining the convergence rate. When $\sum_{k=1}^{i-1} h_{i,k}(x_k \cos\varphi_{i,k} + y_k \sin\varphi_{i,k}) > 0$, other CPG units will enhance the connection signal of the ith CPG unit. When $\sum_{k=1}^{i-1} h_{i,k}(x_k \cos\varphi_{i,k} + y_k \sin\varphi_{i,k}) < 0$, other CPG units will inhibit the connection signal of the ith CPG unit. z_i is the output signal of the ith CPG, and c_i is the magnification coefficient of the CPG output.

In practical engineering, the servomotor has the maximum output velocity and angle. When the CPG unit outputs an excessive frequency or amplitude, it is necessary to adjust the output signal. Furthermore, Fig. 6 shows that the CPG network has double chain-type structures, and the coupling relationship between the CPG units is not a strict neighborhood coupling mode. Joint 2, 4, 6, 8 only has a coupling relationship with one adjacent joint. Joint 5, 7 has coupling relationship with two adjacent joints. Joint 1, 3 has coupling relationship with three adjacent joints. Therefore, in view of computer control, the CPG model should be modified and discretized in time domain as

$$
\begin{cases}
\begin{cases}
\text{if } i = 2, 4, 6, 8 \\
\frac{x_i[j]-x_i[j-1]}{\Delta T} = -\omega_i y_i[j] + x_i[j](m_i - x_i[j]^2 - y_i[j]^2) + h_{i,i-1}(x_{i-1}[j]\cos\varphi_{i,i-1} + y_{i-1}[j]\sin\varphi_{i,i-1}) \\
\frac{y_i[j]-y_i[j-1]}{\Delta T} = \omega_i x_i[j] + y_i[j](m_i - x_i[j]^2 - y_i[j]^2)
\end{cases} \\
\begin{cases}
\text{if } i = 5, 7 \\
\frac{x_i[j]-x_i[j-1]}{\Delta T} = -\omega_i y_i[j] + x_i[j](m_i - x_i[j]^2 - y_i[j]^2) + h_{i,i-4}(x_{i-4}[j]\cos\varphi_{i,i-4} + y_{i-4}[j]\sin\varphi_{i,i-4}) \\
\frac{y_i[j]-y_i[j-1]}{\Delta T} = \omega_i x_i[j] + y_i[j](m_i - x_i[j]^2 - y_i[j]^2) + h_{i,i+1}(x_{i+1}[j]\cos\varphi_{i,i+1} + y_{i+1}[j]\sin\varphi_{i,i+1})
\end{cases} \\
\begin{cases}
\text{if } i = 1 \\
\frac{x_i[j]-x_i[j-1]}{\Delta T} = -\omega_i y_i[j] + x_i[j](m_i - x_i[j]^2 - y_i[j]^2) + h_{i,i+4}(x_{i+4}[j]\cos\varphi_{i,i+4} + y_{i+4}[j]\sin\varphi_{i,i+4}) \\
\qquad + h_{i,i+2}(x_{i+2}[j]\cos\varphi_{i,i+2} + y_{i+2}[j]\sin\varphi_{i,i+2}) \\
\frac{y_i[j]-y_i[j-1]}{\Delta T} = \omega_i x_i[j] + y_i[j](m_i - x_i[j]^2 - y_i[j]^2) + h_{i,i+1}(x_{i+1}[j]\cos\varphi_{i,i+1} + y_{i+1}[j]\sin\varphi_{i,i+1})
\end{cases} \\
\begin{cases}
\text{if } \quad i = 3 \\
\frac{x_i[j]-x_i[j-1]}{\Delta T} = -\omega_i y_i[j] + x_i[j](m_i - x_i[j]^2 - y_i[j]^2) + h_{i,i+4}(x_{i+4}[j]\cos\varphi_{i,i+4} + y_{i+4}[j]\sin\varphi_{i,i+4}) \\
\qquad + h_{i,i-2}(x_{i-2}[j]\cos\varphi_{i,i-2} + y_{i-2}[j]\sin\varphi_{i,i-2}) \\
\frac{y_i[j]-y_i[j-1]}{\Delta T} = \omega_i x_i[j] + y_i[j](m_i - x_i[j]^2 - y_i[j]^2) + h_{i,i+1}(x_{i+1}[j]\cos\varphi_{i,i+1} + y_{i+1}[j]\sin\varphi_{i,i+1})
\end{cases} \\
z_i[j] = \begin{cases} c_i y[j], & \text{if } |z_i[j] - z_i[j-1]| \le ST \\ z_i[j-1] + ST, & \text{if } z_i[j] - z_i[j-1] > ST \\ z_i[j-1] - ST, & \text{if } z_i[j] - z_i[j-1] < -ST \end{cases}, i = 1, 2, ...8 \\
z_i[j] = \begin{cases} c_i y[j], & \text{if } |z_i[j]| \le A \\ A, & \text{if } z_i[j] > A \\ -A, & \text{if } z_i[j] < -A \end{cases}, i = 1, 2, ...8
\end{cases}
\tag{13}
$$

https://doi.org/10.1017/S0263574718000590 Published online by Cambridge University Press

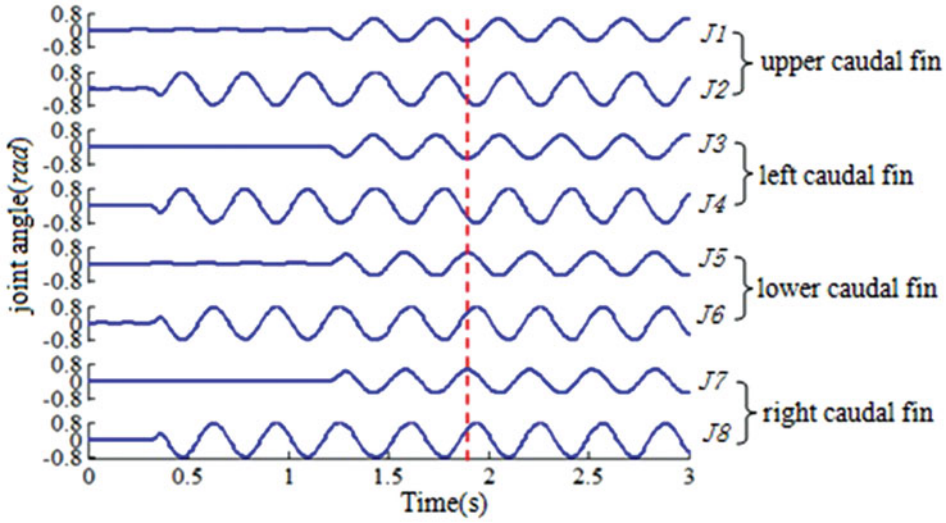


Fig. 7. CPG output signals for oscillating joints in undulation propulsion mode.

where $x_i[j]$ and $y_i[j]$ are the membrane potential and adjusting potential of the ith CPG unit at j moment, respectively. $z_i[j]$ is the output signal of the ith CPG unit at j moment. ΔT is the discrete time step. S is the maximum angular velocity of the servomotor. $T = 20$ ms is the period of PWM signal, and A is the maximum output angular displacement of the servo actuator.

4.3. CPG-based control for undulation and jet propulsion movement

In order to ensure the symmetric motions, the four caudal fins should share the same CPG control parameters of frequency ω_i and amplitude m_i in the corresponding joint. In addition, the joints in the face-to-face installed caudal fins should have a phase difference of 180°.

As mentioned in Section 2.2, when the four caudal fins of the BUR conduct carangiform fish-like undulation movement simultaneously, the BUR can overall achieve the undulation propulsion movement. Observations in nature indicate that fish swimming is usually accompanied by a backward-moving propulsive wave that travels along the caudal fin. Like a carangiform swimmer, when the amplitude of the body wave is limited anteriorly and then increases in the posterior half of the body, thrust is mainly generated by the caudal fin. To replicate carangiform fish-like undulate swimming, we created a backward-moving propulsive wave featured by increasing amplitude and phase lag by configuring and adjusting the control parameters of the CPG model. Figure 7 shows an example of CPG-governed undulation propulsion movement, and the CPG parameter values for undulation propulsion movement are listed in Table II. As can be seen, taking the J_1 and J_2 in upper caudal fin as examples, when the output CPG oscillator signals have constant frequency and amplitude (such as the time show in the red vertical dashed line), the CPG signal fed to J_1 has smaller amplitude and earlier phase. Furthermore, the CPG signals fed to the joints in upper caudal fin are similar to that in left caudal fin but opposite in phase to that in lower and right caudal fin.

Jet propulsion movement is featured by a high-speed backward jet flow formed in the rear of the body. Observations in jellyfish show that jellyfish rapidly shrinks its outer membrane to extrude the water in the lumen, and then a backward jet flow is formed, which generates a reactive force to push the jellyfish move forward. To imitate the jellyfish-like swimming, we created a backward jet flow by rapidly folding four caudal fins to extrude the water among the caudal fins. Figure 8 gives an example of CPG-governed jet propulsion movement, and the corresponding CPG parameters are as shown in Table III, which indicates there is no CPG signal fed to *J2*, *J4*, *J6* and *J8*. The CPG signal fed to *J1* is similar to that to *J3* but opposite in phase to *J5* and *J7*. Due to different speed configurations between the outspread fins stage and fold fins stage, the CPG output signals are no longer sinusoidal.

Figure 9 illustrates the effects of BUR control parameters on its CPG output signals. When the characteristic parameters are adjusted abruptly, the CPG output signals can be switched to another stable oscillation state quickly and smoothly. Thus, the CPG-based control method can offers a worthwhile avenue to the problem of gait transitions.

https://doi.org/10.1017/S0263574718000590 Published online by Cambridge University Press

Table II. CPG parameters for undulation propulsion mode.

m_1	m_2	m_3	m_4	m_5	m_6	m_7	m_8	ω_i	c_i
3	6	3	6	3	6	3	6	2	1/3

$$\mathbf{h} = \begin{bmatrix} 0 & 1 & 1 & 0 & 1 & 0 & 0 & 0 \\ 1 & 0 & 0 & 0 & 0 & 0 & 0 & 0 \\ 1 & 0 & 0 & 1 & 0 & 0 & 1 & 0 \\ 0 & 0 & 1 & 0 & 0 & 0 & 0 & 0 \\ 1 & 0 & 0 & 0 & 0 & 1 & 0 & 0 \\ 0 & 0 & 0 & 0 & 1 & 0 & 0 & 0 \\ 0 & 0 & 1 & 0 & 0 & 0 & 0 & 1 \\ 0 & 0 & 0 & 0 & 0 & 0 & 1 & 0 \end{bmatrix} \quad \varphi = \begin{bmatrix} * & \pi/6 & 0 & * & \pi & * & * & * \\ \pi/6 & * & * & * & * & * & * & * \\ 0 & * & * & \pi/6 & * & * & \pi & * \\ * & * & \pi/6 & * & * & * & * & * \\ \pi & * & * & * & * & \pi/6 & * & * \\ * & * & * & * & \pi/6 & * & * & * \\ * & * & \pi & * & * & * & * & \pi/6 \\ * & * & * & * & * & * & \pi/6 & * \end{bmatrix}$$

Note: "*" indicates that there is no relative motion between the joints.

Table III. CPG parameters for jet propulsion mode.

m_1	m_2	m_3	m_4	m_5	m_6	m_7	m_8	ω_{i1}	ω_{i2}	c_i
4	40	4	40	4	40	4	40	1	3	1/3

$$\mathbf{h} = \begin{bmatrix} 0 & 1 & 1 & 0 & 1 & 0 & 0 & 0 \\ 1 & 0 & 0 & 0 & 0 & 0 & 0 & 0 \\ 1 & 0 & 0 & 1 & 0 & 0 & 1 & 0 \\ 0 & 0 & 1 & 0 & 0 & 0 & 0 & 0 \\ 1 & 0 & 0 & 0 & 0 & 1 & 0 & 0 \\ 0 & 0 & 0 & 0 & 1 & 0 & 0 & 0 \\ 0 & 0 & 1 & 0 & 0 & 0 & 0 & 1 \\ 0 & 0 & 0 & 0 & 0 & 0 & 1 & 0 \end{bmatrix} \quad \varphi = \begin{bmatrix} * & 0 & 0 & * & \pi & * & * & * \\ 0 & * & * & * & * & * & * & * \\ 0 & * & * & 0 & * & * & \pi & * \\ * & * & 0 & * & * & * & * & * \\ \pi & * & * & * & * & 0 & * & * \\ * & * & * & * & 0 & * & * & * \\ * & * & \pi & * & * & * & * & 0 \\ * & * & * & * & * & * & 0 & * \end{bmatrix}$$

Note: ω_{i1} and ω_{i2} indicate the frequency parameters in outspread and fold caudal fins stage, respectively. "*" indicates that there is no relative motion between the joints.

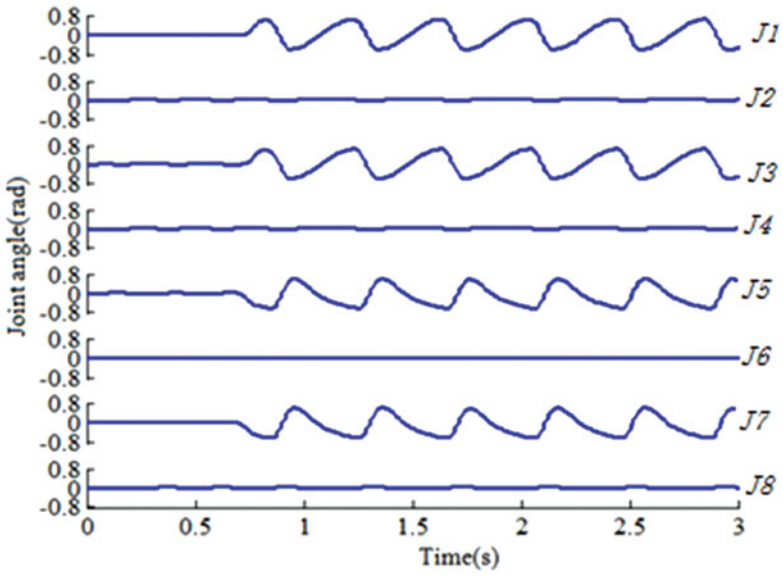


Fig. 8. CPG output signals for oscillating joints in jet propulsion mode.

5. Experiments and Results

In this study, a series of aquatic experiments were reported to highlight the proposed swimming control methods for the BUR, and particularly to compare the kinematic characteristics between undulation propulsion mode and jet propulsion mode.

https://doi.org/10.1017/S0263574718000590 Published online by Cambridge University Press

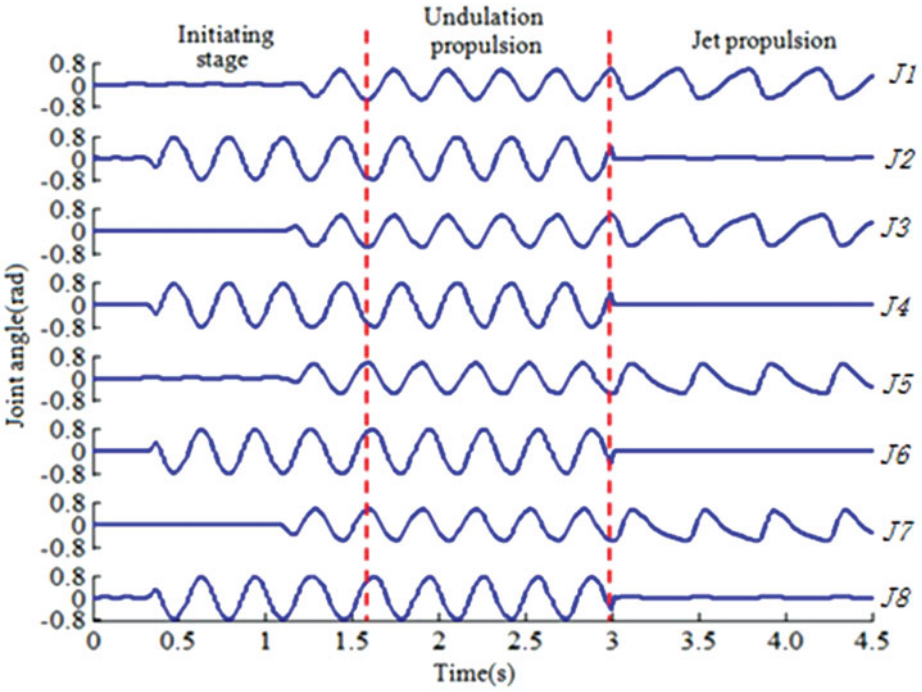


Fig. 9. CPG output signals in gait transitions.

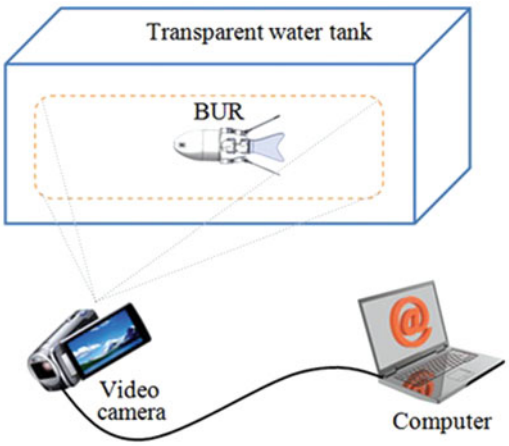


Fig. 10. Linear velocity testing platform.

5.1. Experimental procedure

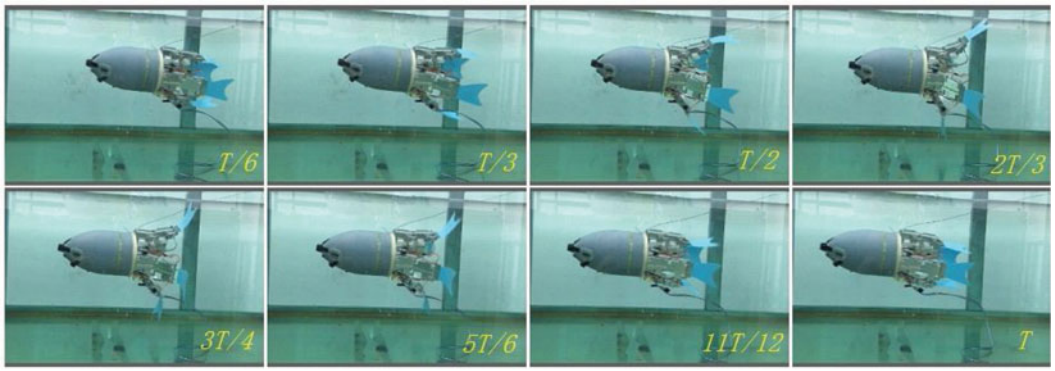
Experiments were conducted to investigate the effects of the key caudal fin actuation parameters on its linear swimming velocity. According to the CPG-govern model, two controllable caudal fin actuation parameters were chosen in these experiments: caudal fin actuation frequency and amplitude. As shown in Fig. 10, a test platform was developed to measure the swimming velocity. The platform is composed a 3 m × 2 m × 1 m (length × width × depth) transparent water tank, a high dynamic range video camera and a computer. To measure the swimming velocity, the BUR was filmed by the high dynamic range video camera when performing linear swimming in the water tank. The velocity of the BUR in each test was calculated according to the measured distance traveled and the corresponding time taken. Each test was conducted for three times and the average velocity was calculated based on the three test results.

Figure 11 shows a snapshot sequence of undulation propulsion mode and jet propulsion mode in a swimming period T. At the beginning, the BUR normally swam forwards in the jet propulsion mode

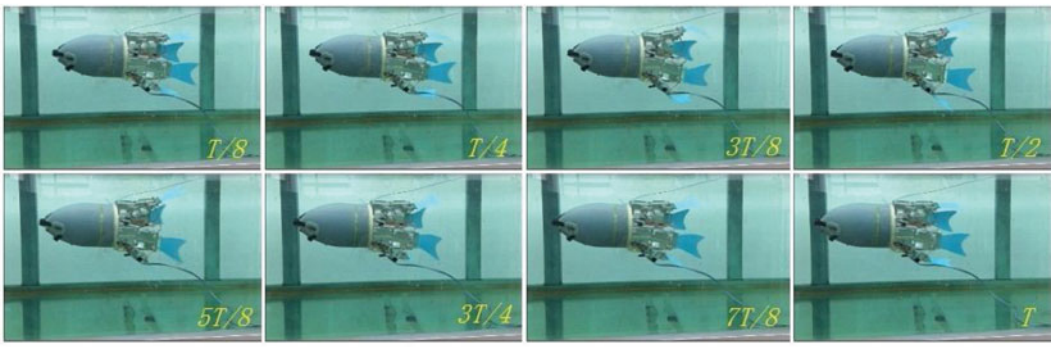
https://doi.org/10.1017/S0263574718000590 Published online by Cambridge University Press

Table IV. Commanded caudal fin actuation parameters for linear swimming.

Case	Propulsion mode	f (Hz)	A (cm)
1	Jet propulsion	0.5, 0.6, 0.8, 1.3, 2.5	13
2		1.3	6, 9, 11, 13, 15
3	Undulation propulsion	0.5, 0.6, 0.8, 1.3, 2.5	13
4		1.3	6, 9, 11, 13, 15



(a)



(b)

Fig. 11. Snapshot sequence of linear swimming. (a) Jet propulsion movement ($m_1 = m_3 = m_5 = m_7 = 4, m_2 = m_4 = m_6 = m_8 = 40, \omega_{i1} = 1, \omega_{i2} = 3$). (b) Undulation propulsion movement ($m_1 = m_3 = m_5 = m_7 = 3, m_2 = m_4 = m_6 = m_8 = 5, \omega_i = 3$).

(as shown in Fig. 11(a)) and then smoothly switched to the undulation propulsion mode (as shown in Fig. 11(b)) when the CPG parameters were changed abruptly.

5.2. Results and discussion

In this section, we compared the kinematic characteristics of the BUR in undulation propulsion mode and jet propulsion mode. Four sets of experiments were performed to obtain the linear swimming velocity. The commanded caudal fin actuation parameters are listed in Table IV. During the test, unless otherwise specified, the data points and error bars in figures were the averages and standard deviations of three runs, respectively.

The linear swimming velocities as a function of caudal fin actuation frequency and amplitude are shown in Fig. 12(a) and (b) , respectively. To investigate the effects of BUR propulsion mode on its velocity, velocities in undulation propulsion mode and jet propulsion mode were plotted on each graph. As can be seen from Fig. 12(a), the swimming velocity initially increased rapidly with the frequency and then slowed down when the frequency was greater than 0.8 Hz in both propulsion modes. There are two possible reasons for this trend. One reason could be the effect of drag. The BUR suffered a thrust force from the caudal fin and a drag force from the fluid simultaneously. The thrust

https://doi.org/10.1017/S0263574718000590 Published online by Cambridge University Press

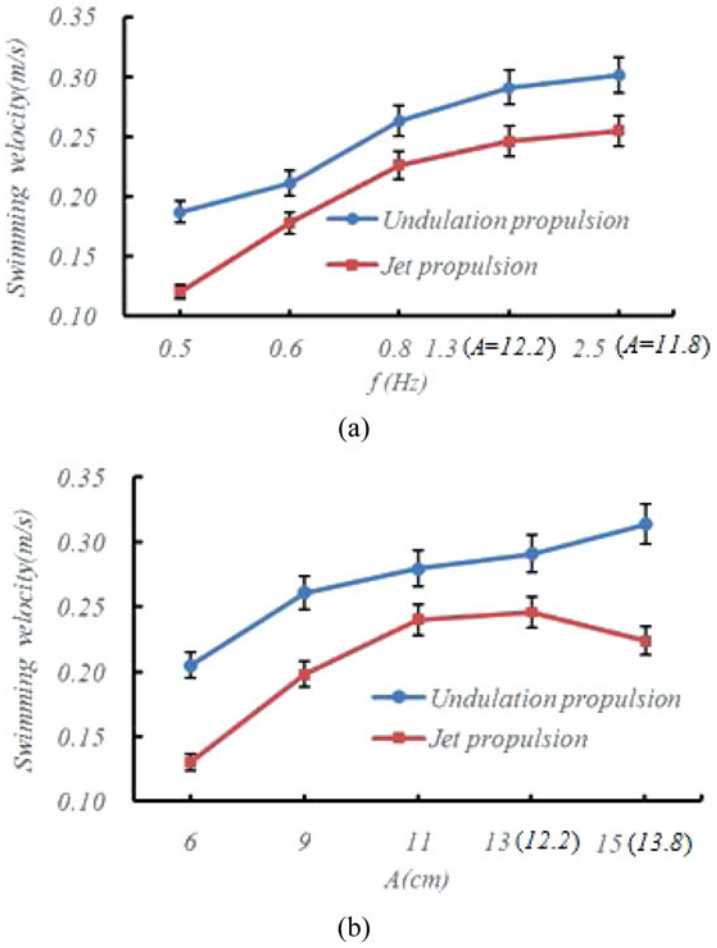


Fig. 12. Swimming velocities as a function of (a) frequency at $A = 13$ cm and (b) amplitude at $f = 1.3$ Hz.

force increased with frequency, but the drag force increased with the swimming velocity as well.[32] When the BUR reached to a certain velocity, the effects of drag were significant. Therefore, the growth in net force decelerated and the growth speed of the swimming velocity declined. The other reason is the speed limit of the servomotor. The desired amplitudes ($A = 13$, 15 cm) cannot be achieved at high frequencies ($f = 1.3$, 2.5 Hz). The actual amplitudes are labeled next to the commanded amplitudes on the axis of the figures. Therefore, the swimming velocity of the BUR cannot meet the desired value. In addition, the velocities in undulation propulsion mode were higher than that in jet propulsion mode under the same caudal fin actuation parameters. The maximum velocity was up to 0.32 m·s^{-1} (0.53 Body length per second, BL·s^{-1}) at a frequency of 1.3 Hz and an amplitude of 15 cm in the undulation propulsion mode. Figure 12(b) shows the velocity as a function of the amplitude. As can be seen, the swimming velocity in the undulation propulsion mode increased with the amplitude in the measurement ranges. However, the swimming velocity in the jet propulsion mode initially increased quickly with the amplitude and then kept constant and even decreased when the amplitude was greater than 11 cm. The possible reason for this phenomenon is that the BUR suffered a backward force in caudal fin outspread stage and a thrust force in caudal fin fold stage. Both backward force and thrust force increased with the amplitude. When the caudal fin actuation amplitude reached a specific value, the backward force increased faster than the thrust force. Therefore, the swimming velocity declined as the amplitude increased.

A series of performance parameters are listed in Table V to make a compare with other notable works. As can be seen, under the similar size and swimming parameters, the BUR can achieve a higher speed in the same propulsion mode. Furthermore, the BUR has two propulsion modes, which has better environmental adaptability.

https://doi.org/10.1017/S0263574718000590 Published online by Cambridge University Press

Table V. Performance parameters comparison.

Prototype	Size ($L \times W \times H$) (mm)	Propulsion mode	Frequency (Hz)	Amplitude (cm)	Speed ($BL{\cdot}s^{-1}$)
Biomimetic Mantle Jet Propeller[33]	600×170×70	Undulatory	1.4	12	0.25
Multi-Joint Robotic Fish[34]	250×160×70	Jetting	0.83	–	0.35
BUR	600×170×170	Undulatory	1.3	15	0.53
		Jetting	0.8	13	0.37

6. Conclusion

Inspired by both carangiform fish and jellyfish, a novel type of BUR with multi-flexible caudal fins was proposed in this paper. We endeavored to combine the undulation propulsion mode and jet propulsion mode in the self-propelled BUR. First, the prototype design and swimming strategy of the BUR were discussed. Based on the simplified mechanical model of the BUR, a dynamic model of the caudal fins was established. Subsequently, a CPG model was proposed to generate the undulation propulsion mode and jet propulsion mode. A discrete control equation including various constraint conditions was given. Finally, a series of comparative experiments on the BUR were presented. The BUR achieved a maximum swimming velocity of 0.32 $m{\cdot}s^{-1}$ at the frequency of 1.3 Hz and the amplitude of 15 cm in undulation propulsion mode. Furthermore, the swimming stability and cruise performance of the BUR were reviewed. The experimental results indicate that the BUR exhibits stable multi-propulsion modes and it is suitable for complex underwater environment tasks. This paper only focus on the undulation and jet propulsion control; the braking, turning, emerging and submerging movements will be studied in a future work.

Acknowledgment

This research is financially supported by Science and Technology Planning Project of Suzhou, China (Grant no. SNG2017054), Cooperative Innovation Fund-Prospective of Jiangsu Province (BY2016044-01) and Natural Science Foundation of Suzhou Science and Technology University (Grant no. XKQ201609).

References

1. Y. S. Ryuh, G. H. Yang and J. D. Liu, "A school of robotic fish for mariculture monitoring in the sea coast," *J. Bionic Eng.* **12**, 37–46 (2015).
2. P. E. Sitorus, Y. Y. Nazaruddin and E. Leksono "Design and implementation of paired pectoral fins locomotion of labriform fish applied to a fish robot," *J. Bionic Eng.* **6**, 37–45 (2009).
3. S. B. Williams, P. M. Newman and J. Rosenblatt, "Autonomous underwater navigation and control," *Robotica* **19**, 481–496 (2011).
4. P. R. Bandyopadhyay, "Trends in biorobotic autonomous undersea vehicles," *IEEE J. Ocean. Eng.* **30**, 109–139 (2005).
5. L. Lionel, "Underwater robots part I: Current systems andproblem pose," **In:** *Mobile Robotics Towards New Applications* (A. Lazinica, ed.) (InTech Open, Austria/Germany, 2006) pp. 335–360.
6. P. R. Bandyopadhyay, D. N. Beal and A. Menozzi, "Biorobotic insights into how animals swim," *J. Exp. Biol.* **211**, 206–214 (2008).
7. B. G. Tong and L. X. Zhuang, "Hydrodynamic model for undulation swimming of fish and its application," *Chin. J. Nature* **1**, 1–7 (1998).
8. Z. L. Wang, J. Li and G. R. Hang, "Mechanism of jet propulsion in aquatic life and its application to biomimetic jet propulsion vehicles," *Robot* **31**, 281–228 (2009).
9. J. D. Liu and H. S. Hu, "Biological Inspiration: From carangiform fish to multi-joint robotic fish," *J. Bionic Eng.* **7**, 35–48 (2010).
10. P. F. Linden and J. S. Turner, "'Optimal' vortex rings and aquatic propulsion mechanisms," *Proc. R. Soc. B* **271**, 647–653 (2004).
11. M. J. Lighthill, "Note on the swimming of slender fish," *J. Fluids Mech.* **9**, 305–317 (1960).
12. E. J. Anderson and M. E. Demont, "The mechanics of locomotion in the squid *Loligo pealei*: Locomotory function and unsteady hydrodynamics of the jet and intramantle pressure," *J. Exp. Biol.* **203**, 2851–2863 (2000).
13. B. Kim, S. G. Park and W. X. Huang, "Self-propelled heaving and pitching flexible fin in a quiescent flow," *Int. J. Heat Fluid Flow* **62**, 273–281 (2016).

https://doi.org/10.1017/S0263574718000590 Published online by Cambridge University Press

14. D. Xia, W. Chen and Z. J. Wu, "Research on hydrodynamics of carangiform mode robotic fish swimming under self-propulsion," *J. Mech. Eng.* **49**, 54–61 (2013).
15. H. S. Jiang and M. A. Grosenbaugh, "Numerical simulation of vortex ring formation ion the presence of background flow with implications for squid propulsion," *Theor. Comput. Fluid Dyn.* **20**, 103–123 (2006).
16. A. R. Chowdhury, V. Kumar and B. Prasad, "Kinematic study and implementation of a bio-inspired robotic fish underwater vehicle in a Lighthill mathematical framework," *Robot. Biomim.* **1**, 1–16 (2014).
17. T. Salumae and M. Kruusmaa, "A flexible fin with bio-inspired stiffness profile and geometry," *J. Bionic Eng.* **8**, 418–428 (2011).
18. E. L. Blevins and G. V. Lauder, "Rajiform locomotion:Three-dimensional kinematics of the pectoral fin surface during swimming in the freshwater stingray *Potamotrygon orbignyi*," *J. Exp. Biol.* **215**, 3231–3241 (2012).
19. S. Heo, T. Wiguna and H. C. Park, "Effect of an artificial caudal fin on the performance of a biomimetic fish robot propelled by piezoelectric actuators," *J. Bionic Eng.* **4**, 151–158 (2007).
20. P. L. Nguyen, B. R. Lee and K. K. Ahn, "Thrust and swimming speed analysis of fish robot with non-uniform flexible tail," *J. Bionic Eng.* **13**, 73–83 (2016).
21. H. Kim and J. Lee, "Design, swimming motion planning and implementation of a legged underwater robot (CALEB10: D.BeeBot) by biomimetic approach," *Ocean Eng.* **130**, 310–327 (2017).
22. J. Li, Y. L. Guo and Z. L. Wang, "A bionic jellyfish robot propelled by bio-tentacle propulsors actuated by shape memory alloy wires," *J. Harbin Inst. Technol.* **1**, 104–110 (2014).
23. M. Ajallooeian, M. N. Ahmadabadi, B. N. Araabi and H. Moradi, "Design, implementation and analysis of an alternation-based central pattern generator for multidimensional trajectory generation," *Robot. Auton. Syst.* **60**, 182–198 (2012).
24. X. Wu and S. Ma "Adaptive creeping locomotion of a CPG-controlled snake-like robot to environment change," *Auton. Robots* **28**, 283–294 (2010).
25. C. Zhou and K. H. Low "Design and locomotion control of a biomimetic underwater vehicle with fin propulsion," *IEEE/ASME Trans. Mechatron.* **17**, 25–35 (2012).
26. J. Yu, M. Wang, M. Tan and J. Zhang "Three-dimensional swimming," *IEEE Robot. Autom. Mag.* **18**, 47–58 (2011).
27. T. Bajcar *et al.* "Kinematic properties of the jellyfish Aurelia sp," *Jellyfish Blooms*. **2**, 279–289 (2009).
28. C. M. Breder "The locomotion of fishes," *Zoologica*. **4**, 159–297 (1926).
29. P. W. Webb "Form and function in fish swimming," *Sci. Am.* **25**, 58–68 (1984).
30. Z. X. Wu, J. Z. Yu and Z. S. Su, "Control and implementation of S-start for a multijoint biomimetic robotic fish," *Acta Autom. Sin.* **39**, 1915–1922 (2013).
31. M. Wang, J. Z. Yu and M. Tan, "CPG-based multi-modal swimming control for robotic dolphin," *Acta Autom. Sin.* **40**, 1933–1941 (2014).
32. O. M. Curet, N. A. Patankar, G. V. Lauder and M. A. MacIver "Mechanical properties of a bio-inspired robotic knifefish with an undulatory propulsor," *Bioinspir. Biomim.* **6**, 1–9 (2011).
33. Q. Y. Ren, J. X. Xu and L. P. Fan, "A GIM-Based biomimetic learning approach for motion generation of a multi-joint robotic fish," *J. Bionic Eng.* **10**, 423–433 (2013).
34. F. Gao, Z. L. Wang and Y. K. Wang, "A prototype of a biomimetic mantle jet propeller inspired by cuttlefish actuated by SMA wires and a theoretical model for its jet thrust," *J. Bionic Eng.* **11**, 412–422 (2014).

https://doi.org/10.1017/S0263574718000590 Published online by Cambridge University Press